Two-phase electro-magneto-fluid dynamics model and its computational fluid dynamics implementation

Stefan A. Bošković[1] and Branko Bugarski[2]

[1)]*Innovation Center of the Faculty of Technology and Metallurgy in Belgrade Ltd., Karnegijeva 4, 11120 Belgrade, Serbia*

[2)]*University of Belgrade, Faculty of Technology and Metallurgy, Karnegijeva 4, 11120 Belgrade, Serbia*

(*Electronic mail: sboskovic@tmf.bg.ac.rs)

(Dated: 16 January 2024)

In this work, we present a two-phase electro-magneto-fluid dynamics (EMFD) model that merges electromagnetics and fluid dynamics. The model is suitable for use in computational fluid dynamics (CFD) software and was incorporated into OpenFOAM® after deriving appropriate equations that bypassed certain limitations of the software. Currently, there is a lack of even single-phase EMFD models that can be incorporated in CFD software, while simpler models from electrohydrodynamics (EHD) and magnetohydrodynamics (MHD) are being implemented, though they have certain approximations that can limit their applicability. We conclude that the derived EMFD model is applicable and show its quality by implementing it and analyzing the results. We use cases with a droplet and the electrospinning process for verification. The drop deformations obtained were closer to analytical predictions than in the literature for two EHD models, but some oscillations were observed. We compared one simulation to the prediction of an analytical equation from MHD, and good agreement was shown. Finally, we simulate the electrospinning process, and the results were very close to the analytical predictions. We conclude that the implementation can be used for both EHD and MHD cases.

Keywords: electro-magneto-fluid dynamics; EMFD;electrohydrodynamics; magnetohydrodynamics;OpenFOAM®; CFD

NOMENCLATURE

Roman symbols

A magnetic vector potential ($V\,s\,m^{-1}$)

a drop's length measured in the direction that is perpendicular to **E** for EHD or to **B** for MHD cases (m)

B magnetic flux density (T)

b drop's length measured in the direction that is parallel to **E** for EHD or to **B** for MHD cases (m)

Bo Bond number (/)

Co Courant number (/)

D electric displacement ($C\,m^{-2}$)

d diameter (m)

E electric field strength ($V\,m^{-1}$)

F force (N)

g gravitational acceleration ($m\,s^{-2}$)

H magnetic field strength ($A\,m^{-1}$)

J electric current density ($A\,m^{-2}$)

k demagnetizing factor (/)

l length (m)

M magnetization ($A\,m^{-1}$)

P electric polarization ($C\,m^{-2}$)

p pressure (Pa)

Q volumetric flowrate ($m^3\ s^{-1}$)

r radius (m)

t time (s)

$\mathbf{U}$ velocity ($m\ s^{-1}$)

x an axis (/)

Greek symbols

α volume fraction (/)

γ interfacial tension ($N\ m^{-1}$)

Δ deformation (/)

ε electric permittivity ($F\ m^{-1}$)

μ magnetic permeability ($H\ m^{-1}$)

μ_f dynamic viscosity ($Pa\ s$)

ξ eccentricity (/)

ρ mass density ($kg\ m^{-3}$)

ρ_e electric charge density ($C\ m^{-3}$)

σ_e electric conductivity ($S\ m^{-1}$)

ϕ electric potential (V)

Subscripts

0 vacuum

an analytical

b bottom

ct capillary tube

e electric

em electromagnetic

ext external

i fluid *i*, *i*=1,2

j jet

l left

m magnetic

r right

s surface tension

ss steady state

x x-axis

y y-axis

z z-axis

Abbreviations

CFD Computational Fluid Dynamics

EHD ElectroHydroDynamics

EMFD Electro-Magneto-Fluid Dynamics

FVM Finite Volume Method

MHD MagnetoHydroDynamics

VoF Volume of Fluid

I. INTRODUCTION

The influence of electromagnetic fields on fluid flow is studied through electro-magneto-fluid dynamics (EMFD).[1] EMFD is a science that encompasses electrohydrodynamics (EHD) and magnetohydrodynamics (MHD), but it is broader and cannot be obtained as just a sum of EHD and MHD. It is applicable to cases studied in both fields and to more complex cases. Although there is a certain amount of literature about EHD and MHD[2], it is questionable how many applicable software implementations exist today.[3] On the other hand, there is a lack of literature about EMFD, and it can be said that the present state of EMFD is much worse than the state of EHD and MHD. EMFD needs to be established as a field, and the focus should shift from the implementation of EHD and MHD models to the establishment of EMFD. The fact whether electromagnetics and fluid dynamics are merged or not can be used as a gauge of the current state of EMFD.

EMFD does not necessarily have to be created by summing up EHD and MHD. If EMFD is derived solely in this way, certain interaction terms might be absent in the final model. For instance, Ref. 4 illustrates that the electromagnetic force density includes the electric force, the magnetic force, and an additional term. Hence, a better method for the derivation of EMFD may be required. Currently, both fluid dynamics and electromagnetics have been developed enough to enable direct derivation of EMFD from these two fields. This approach was used in this study, and it can be concluded that the resultant EMFD model is derived by using both electromagnetics and fluid dynamics, with the influence of EHD and MHD being minimal (i.e. this EMFD model was not derived as a sum of EHD and MHD).

While the usage of fluid dynamics is relatively straightforward, the situation with electromagnetics is different. Various discussions and theories exist in electromagnetics, leading to different expressions for forces.[5] For example, the theories of Abraham,[6] Minkowski,[7] and Einstein and Laub[8] were proposed more than a century ago, yet none of them were commonly accepted, and new papers have been written since that still lacked common acceptance.[9] Selection of appropriate expressions from electromagnetics is, therefore, more difficult, and their inclusion into EMFD is expected to extend the aforementioned discussions into this field as well. Ref. 9 provides an example that can be linked to EHD, and expressions from that source might be suitable. However, different or better expressions are likely to be discovered as electromagnetics continues to develop. The development of electromagnetics may even be accelerated by EMFD after it is fully established.

Once an EMFD model has been derived, it can be integrated into specific software for practical use. The software implementation process for EHD and MHD can be applied here. For instance, computational fluid dynamics (CFD) has been used for both EHD and MHD calculations, as seen in the literature.[10,11] Therefore, it is reasonable to expect good results for EMFD calculations if CFD is used. This is because EHD and MHD models are expected to be less complex than EMFD models, and some equations present in EMFD models might also be present in EHD or MHD models. Hence, it might be easier and more effective to first implement EHD and MHD models, optimize these implementations, and then use the conclusions from these processes for EMFD model implementation. However, at present, optimized complete EHD and MHD models might not exist. For example, the CFD software called OpenFOAM® only has an MHD model implementation (which is not fully investigated), while EHD model implementations can be found in the literature[12] and an optimization process of EHD implementations was just recently started,[13] so it is still ongoing. An EHD model present in other CFD software called Basilisk, for which it can be said that it is optimized and incomplete (because the electrostrictive force[14] is not included), still cannot be used for full three-dimensional simulations (it can only be used for axially-symmetric simulations), while an MHD model is not present. The second option is to start directly implementing and optimizing EMFD models. The implementation of EMFD models might not be so problematic, but the optimization could be lengthy and problematic because of the number of equations present in the EMFD model in question.

Once the model is implemented, validation is necessary. However, analytical equations from EMFD that can be used for validating EMFD models are not readily available. In such cases, analytical equations from EHD and MHD can be used as alternatives. The most complex set-up for validating EHD software implementations is the one with a drop of one fluid surrounded by another fluid.[15] Two analytical equations are available in EHD for this setup – one for the perfect dielectric model[2] and one for the leaky dielectric model.[15,16] Although theories for this setup have existed for some time, recent theoretical advancements are still available.[17] A qualitative test can also be found for this setup for the leaky dielectric model. However, this test can be influenced by numerical errors at low electric field strengths, so its inclusion is not mandatory if good results are obtained in quantitative comparison with analytical predictions. An analytical equation for this setup can also be found in MHD.[18] Other analytical equations for simpler cases can also be found and can be included in papers focusing not on EMFD but on software implementation. However, some of the already published analytical equations might have been derived from models that have

inappropriate approximations. For instance, an analytical equation from EHD for the pressure jump that can be seen at the interface of two planar fluid layers can be found in Ref. 15. However, this analytical equation does not mention the electrostrictive force[19] that influences the pressure, and hence, it is not suitable for validation. On the other hand, good results obtained for a setup that is even more complex than the mentioned set-up with a drop could more obviously show the quality of the implementation.

Section II of this paper describes a two-phase EMFD model and explains how it was implemented in the OpenFOAM® CFD software (version 9). The model was simplified and adjusted to be compatible with the software. The solver used for two incompressible and isothermal immiscible fluids (interFoam), which uses the Finite Volume Method (FVM)[20,21] and the Volume of Fluid (VoF) method,[22,23] was chosen as the starting point. The model is suitable for 1D, 2D, and 3D (including full 3D) simulations and can be used for both laboratory and industrial scale applications. It is particularly useful for chemical engineering processes, such as electrospraying[24–26] and electrospinning.[27] This EMFD model is the first implementable and widely applicable one of its kind. It can be used for both perfect dielectrics and leaky dielectrics from EHD (following from Ref. 15), making it a valuable contribution to the field. The model's applicability for EHD was validated by comparing it with two analytical equations from EHD in subsection III A 1, where a deformation of a drop surrounded by another fluid is caused by an electric field. The implementation was even compared with predictions of both analytical equations for the drop deformation from EHD. The implementation's applicability to non-EHD cases was validated in subsection III A 2 using another example with a drop, where a comparison with an analytical equation from MHD is presented. Finally, the paper presents results of simulating the electrospinning process and comparisons with analytical predictions. This is an important contribution as there are few studies on its simulation.[28]

II. MATHEMATICAL MODEL

Out of the equations that were already present in the starting solver, only the Navier-Stokes equation was expanded by placing additional volumetric forces in the appropriate place:[13]

$$\frac{\partial(\rho\mathbf{U})}{\partial t}+\nabla\cdot(\rho\mathbf{U}\mathbf{U})-\nabla\cdot\left(\mu_f\nabla\mathbf{U}\right)=\rho\mathbf{g}-\nabla p+\mathbf{F_s}+\mathbf{F_e}+\mathbf{F_m}+\mathbf{F_{em}} \tag{1}$$

where ρ represents the mass density, $\mathbf{U}$ is the velocity, t the time, μ_f is the dynamic viscosity, $\mathbf{g}$ represents the gravitational acceleration, p the pressure, and $\mathbf{F}$ represents the force, while subscripts s, e, m, and em denote surface tension, electric, magnetic, and electromagnetic, respectively. Other underlying expressions from the starting solver were not modified, for example the surface tension force calculation that can be found in Refs. 29 and 30.

The expressions for $\mathbf{F_e}$, $\mathbf{F_m}$, and $\mathbf{F_{em}}$ were taken from Ref. 9:

$$\mathbf{F_e} = \rho_e \mathbf{E} + \sum_{k=\mathrm{x,y,z}} \left(|\mathbf{P}_k| \nabla \left| \mathbf{E}_{\mathbf{ext},k} \right| \right) \tag{2}$$

$$\mathbf{F_m} = \mathbf{J} \times \mathbf{B} + \sum_{k=\mathrm{x,y,z}} \left(|\mathbf{M}_k| \nabla \left| \mathbf{B}_{\mathbf{ext},k} \right| \right) \tag{3}$$

$$\mathbf{F_{em}} = \frac{\partial}{\partial t} \left(\mathbf{P} \times \mathbf{B_{ext}} \right) \tag{4}$$

where ρ_e represents the electric charge density, $\mathbf{E}$ represents the electric field strength, $\mathbf{P}$ is the electric polarization, $\mathbf{J}$ the electric current density, $\mathbf{B}$ the magnetic flux density, and $\mathbf{M}$ represents the magnetization, while the subscript ext denotes the external, and subscripts x, y, and z denote the corresponding axes. According to Ref. 9, the equations (2)–(4) were derived from an expression that applies to any electromagnetic field and a linear isotropic magnetic dielectric medium. Ref. 9 also provides examples of how this expression can be used, including a parallel-plate capacitor.

The electric field strength[31] is equal to:

$$\mathbf{E} = \mathbf{U} \times \mathbf{B} - \frac{\partial \mathbf{A}}{\partial t} - \nabla \phi \tag{5}$$

where $\mathbf{A}$ and ϕ are the magnetic vector potential and the electric potential, respectively, while the external electric field strength[9] is:

$$\mathbf{E_{ext}} = \mathbf{E} + \frac{\mathbf{P}}{3\varepsilon_0} \tag{6}$$

where ε represents the electric permittivity, while the subscript 0 denotes the vacuum.

The electric polarization[9] is equal to:

$$\mathbf{P} = (\varepsilon - \varepsilon_0)\, \mathbf{E} \tag{7}$$

The electric displacement ($\mathbf{D}$)[9] is given by:

$$\mathbf{D} = \varepsilon \mathbf{E} \tag{8}$$

while its divergence[9,15] is:

$$\nabla \cdot \mathbf{D} = \nabla \cdot (\varepsilon \mathbf{E}) = \rho_e \tag{9}$$

After substituting Eq. (5) into Eq. (9), the following can be derived:

$$\nabla \cdot [\varepsilon (\mathbf{U} \times \mathbf{B})] - \nabla \cdot (\varepsilon \nabla \phi) - \nabla \cdot \left(\varepsilon \frac{\partial \mathbf{A}}{\partial t} \right) = \rho_e \tag{10}$$

The electric current density[15] is equal to:

$$\mathbf{J} = \sigma_e \mathbf{E} + \rho_e \mathbf{U} \tag{11}$$

where σ_e is the electric conductivity.

Starting from:[15]

$$\frac{\partial \rho_e}{\partial t} + \nabla \cdot \mathbf{J} = 0 \tag{12}$$

the following can be obtained after substituting Eqs. (11) and (5):

$$\frac{\partial \rho_e}{\partial t} + \nabla \cdot (\rho_e \mathbf{U}) = \nabla \cdot (\sigma_e \nabla \phi) + \nabla \cdot \left[\sigma_e \left(\frac{\partial \mathbf{A}}{\partial t} - \mathbf{U} \times \mathbf{B} \right) \right] \tag{13}$$

The magnetic flux density[32] is equal to:

$$\mathbf{B} = \nabla \times \mathbf{A} \tag{14}$$

while its divergence[9] is:

$$\nabla \cdot \mathbf{B} = 0 \tag{15}$$

and the external magnetic flux density[9] is:

$$\mathbf{B_{ext}} = \mathbf{B} - \frac{2}{3} \mu_0 \mathbf{M} \tag{16}$$

where μ is the magnetic permeability.

The magnetization[9] is:

$$\mathbf{M} = \left(\frac{\mu}{\mu_0} - 1 \right) \mathbf{H} \tag{17}$$

where $\mathbf{H}$ represents the magnetic field strength.

The magnetic field strength[9] is given by:

$$\mathbf{H} = \frac{\mathbf{B}}{\mu} \tag{18}$$

while its curl[9] is:

$$\nabla \times \mathbf{H} = \frac{\partial \mathbf{D}}{\partial t} + \mathbf{J} \tag{19}$$

If Eqs. (8), (18), and (14) are substituted into Eq. 19, the following can be derived:

$$\begin{aligned} \frac{1}{\mu}\nabla(\nabla\cdot\mathbf{A}) - \nabla\cdot\left(\frac{1}{\mu}\nabla\mathbf{A}\right) + \nabla\mathbf{A}\cdot\nabla\left(\frac{1}{\mu}\right) + \nabla\left(\frac{1}{\mu}\right)\times\mathbf{B} + \frac{\partial}{\partial t}(\varepsilon\nabla\phi) \\ + \frac{\partial}{\partial t}\left(\varepsilon\frac{\partial\mathbf{A}}{\partial t}\right) - \frac{\partial}{\partial t}[\varepsilon(\mathbf{U}\times\mathbf{B})] = \mathbf{J} \end{aligned} \tag{20}$$

Eq. (20) is in this form because the gradient and the curl of a variable cannot be implicitly solved with the OpenFOAM® software.

The Coulomb gauge[32,33] is given by:

$$\nabla\cdot\mathbf{A} = 0 \tag{21}$$

and was used to simplify Eqs. (10) and (20) into:

$$\nabla\cdot[\varepsilon(\mathbf{U}\times\mathbf{B})] - \nabla\cdot(\varepsilon\nabla\phi) - \frac{\partial\mathbf{A}}{\partial t}\cdot\nabla\varepsilon = \rho_e \tag{22}$$

$$\begin{aligned} -\nabla\cdot\left(\frac{1}{\mu}\nabla\mathbf{A}\right) + \nabla\mathbf{A}\cdot\nabla\left(\frac{1}{\mu}\right) + \nabla\left(\frac{1}{\mu}\right)\times\mathbf{B} + \frac{\partial}{\partial t}(\varepsilon\nabla\phi) \\ + \frac{\partial}{\partial t}\left(\varepsilon\frac{\partial\mathbf{A}}{\partial t}\right) - \frac{\partial}{\partial t}[\varepsilon(\mathbf{U}\times\mathbf{B})] = \mathbf{J} \end{aligned} \tag{23}$$

For the VoF method, the standard equations used for calculating the electric permittivity, the electric conductivity, and the magnetic permeability[29] are given by:

$$\varepsilon = \alpha_1\varepsilon_1 + \alpha_2\varepsilon_2 \tag{24}$$

$$\sigma_e = \alpha_1 \sigma_{e1} + \alpha_2 \sigma_{e2} \tag{25}$$

$$\mu = \alpha_1 \mu_1 + \alpha_2 \mu_2 \tag{26}$$

where α represents the volume fraction, while the subscript i, i=1,2 denotes the fluid i. In the software used for the simulation (OpenFOAM®), it was not possible to use complex numbers as required. As a result, real numbers were used in all calculations. In addition, certain boundary conditions between phases were not included, like in other works[10] that made use of the VoF method and OpenFOAM®.

The Courant number (Co) is an important parameter used in CFD simulations to determine time steps. In this study, the electric Courant number[13] was calculated using the following expression:

$$Co_e = \frac{|\mathbf{E}| \sqrt{\varepsilon/\rho}}{\delta x/\delta t} \tag{27}$$

where x is an axis. Starting from the Alfvén-Courant number,[34] an expression for the magnetic Courant number was derived using dimensional analysis:

$$Co_m = \frac{|\mathbf{B}| / \sqrt{\mu\rho}}{\delta x/\delta t} \tag{28}$$

In the OpenFOAM®, the Courant number is a crucial parameter used in the starting solver. To accurately determine the time steps, additional expressions for the interface electric Courant number and the interface magnetic Courant number were derived and used. This resulted in a total of six Courant numbers being used to ensure precise calculations.

In summary:

- Eqs. (1)–(4) are the Navier-Stokes equation and the expressions for the newly added forces
- It can be said that Eqs. (5)–(13) primarily describe the electric field, while Eqs. (14)–(20) describe the magnetic field
- Eqs. (21)–(23) are simplifications
- Eqs. (24)–(26) are used to account for the fact that there are two fluids

Two-phase electro-magneto-fluid dynamics model and its computational fluid dynamics implementation

- The integration of electromagnetics and fluid dynamics can more easily be seen by the presence of $\mathbf{F_e}$, $\mathbf{F_m}$, and $\mathbf{F_{em}}$ in Eq. (1) and by the presence of $\mathbf{U}$ in Eqs. (5), (10), (11), (13), (20), (22), and (23)

To enable the use of these equations, the interFoam solver in OpenFOAM® was expanded. The new solver employs the FVM and the VoF method, just like the previous one. Additionally, new Courant numbers have been introduced in suitable locations based on the existing Courant number and the interface Courant number.

The expressions needed to calculate $\mathbf{F_e}$, $\mathbf{F_m}$, and $\mathbf{F_{em}}$ were added just before the calculation of the velocity and of the pressure starts in a time step in the following way:

- Eqs. (24), (25), and (26) are solved in this order.
- A while loop is started.
  - Eqs. (22), (23), (14), (5), (13), and (11) are solved in this order within this while loop.
- The while loop is ended.
- Eqs. (7), (6), (18), (17), and (16) are solved in this order.
- $\nabla \cdot \mathbf{B}$ is calculated.
- Values of the newly added forces are calculated using Eqs. (2), (3), and (4).

$\mathbf{F_e}$, $\mathbf{F_m}$, and $\mathbf{F_{em}}$ were added to the Navier-Stokes equation in the appropriate place to influence the calculation of the velocity and pressure.

In this implementation of the model, while loops were added to improve the results of interdependent equations. However, it may not be necessary to include them, especially if using low values of time steps in calculations. It is worth noting that a separate while loop for coupled equations was not found in Ref. 15 or in the EHD model implementation in the CFD software Basilisk. Additionally, while the velocity and pressure are interdependent in solvers present in the software OpenFOAM®, and in some of those solvers they are in a loop that can be used in a single time step[35], it is frequently done just once without looping.

III. RESULTS AND DISCUSSION

The simulation involved systems comprising of two different fluids, referred to as fluid 1 and fluid 2. Volume fractions were simulated using the interface compression scheme, and the OpenFOAM® post-processing utility was utilized for determining the interface. The results were displayed and checked using Paraview (and paraFoam). The meshes were static, and dynamic meshes were not employed due to the potential risk of introducing significant numerical errors.[13]

A. Drop deformations

A small droplet of fluid 1 was surrounded by fluid 2. The diameter ($d_{1,t=0}$) of the droplet at the start was 10^{-4} m. Both fluids had the same properties, including mass density (10^3 kg m^{-3}) and kinematic viscosity (10^{-6} m^2 s^{-1}), but the interfacial tension between them was 0.1 N m^{-1}. There was no gravitational acceleration. The electrical permittivity of fluid 1 and fluid 2 was 10^{-10} F m^{-1} and 10^{-11} F m^{-1}, respectively. The electrical conductivity of fluid 1 and fluid 2 was 10^{-7} S m^{-1} and 10^{-12} S m^{-1}, respectively. The magnetic permeability of fluid 1 and fluid 2 was 10^{-4} H m^{-1} and 10^{-6} H m^{-1}, respectively.

After Eq. (26), the new while loop started. It had 100 iterations or would stop earlier if the tolerance and relative tolerance for ϕ, ρ_e, and $\mathbf{A}$ were less than the values used in a single solving of the corresponding equation. A maximum of 100 iterations was chosen to prevent the loop from reaching it in simulations.

In every simulation, the target maximum value for all Courant numbers used was set to 0.1. The simulation time for all systems was 10^{-3} s, with results outputted every 10^{-5} s. The maximum time step was also set to 10^{-5} s. In cases where either ϕ was set to be fixed and different from 0 or $\mathbf{A}$ from $\mathbf{0}$ on two borders, 10^{-5} s was used for the starting value of the first time step. This value was chosen to facilitate checking the applicability of newly added Courant numbers. In cases where ϕ was set to be equal to 0 and $\mathbf{A}$ to $\mathbf{0}$ on two borders, 10^{-7} s was used as the starting value for the first time step because Courant numbers could not affect it.

The possible deformation of a drop of fluid 1 was calculated using:[18,36,37]

$$\Delta_1 = \frac{b-a}{b+a} \tag{29}$$

where Δ represents the deformation, while b and a represent the drop's length measured in

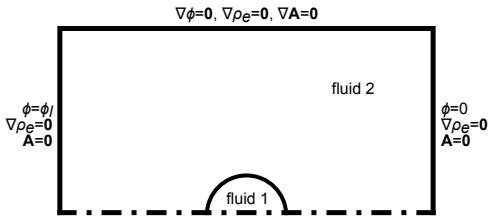

FIG. 1. An illustration of the axially symmetric geometry

the direction that is parallel and perpendicular to **E** for EHD or **B** for MHD cases, respectively. Spherically shaped objects using the VoF method require a mesh with around twenty cells per object diameter for satisfactory results.[22]

1. Axially symmetric cases

Fig. 1 illustrates the geometry used in the simulation. The symmetry axis was located at the bottom, while the left, right, and top borders were walls. In this case, the electric potential on the right border (ϕ_r) was set to 0, while the electric potential on the left border (ϕ_l) was varied. Although a full three-dimensional simulation can be done, geometries employing symmetry are commonly found in literature.[15]

The mesh consisted of hexahedra and prisms, with the height and width of all cells being equal.

The magnitude of the macroscopically uniform electric field strength ($\mathrm{E_{mu}}$) was calculated using the expression written as:

$$|\mathbf{E_{mu}}| = \left| \frac{\phi_\mathrm{l} - \phi_\mathrm{r}}{l_\mathrm{lr}} \right| \tag{30}$$

where l_lr is the length from the left wall to the right wall.

a. Comparison with the perfect dielectric model An analytical equation from literature can be used for comparison with the perfect dielectric model:[2,36]

$$\Delta_{1,ss,an} = \frac{9}{16} \frac{r_{1,t=0}\varepsilon_2}{\gamma} \left(|\mathbf{E_{mu}}| \frac{\varepsilon_1/\varepsilon_2 - 1}{\varepsilon_1/\varepsilon_2 + 2} \right)^2 \tag{31}$$

where $r_{1,t=0}$ represents the starting drop radius, γ represents the interfacial tension. The subscript *ss* denotes the steady state, while the subscript *an* denotes the analytical value.

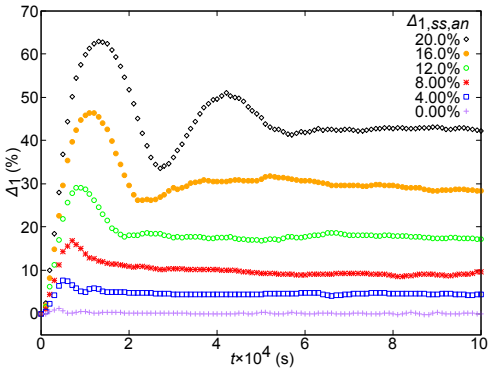

FIG. 2. Numerically obtained drop deformations for cases with different analytical predictions for comparison with the perfect dielectric model

To avoid possible division by zero, the electric conductivities of both fluids were set to be equal to 10^{-100} S m^{-1}, and magnetic permeabilities were set to 10^{-100} H m^{-1}. Additionally, the software OpenFOAM® includes a variable called "small" which can be included in certain equations in possibly problematic places.

The quality of the mesh was analyzed in the subsection with the leaky dielectric model. This analysis used fifty cells per the starting drop diameter. The width and the height of the geometry were five times greater than the starting drop diameter and the starting drop radius, respectively.

Fig. 2 shows a comparison between the obtained results and the corresponding analytical predictions. As expected, there is a difference between the obtained drop deformations and $\Delta_{1,ss,an}$. This discrepancy is due to the fact that the approach used to derive Eq. (31) is only valid for small deformations, small electric fields and steady-state conditions, as stated in Ref. 36. It was not possible to find a method to calculate the correct divergence from this equation in the literature. Therefore, it is also expected that the divergence from Eq. (31) increases as $\Delta_{1,ss,an}$ increases. For lower values of $\Delta_{1,ss,an}$, the closeness of Δ_1 and $\Delta_{1,ss,an}$ is similar to what can be seen in Ref. 36 in Fig. 7a. However, near the end of the presented results, when $\Delta_{1,ss,an}$ was equal to 12.0%, the ratio of Δ_1 and $\Delta_{1,ss,an}$ was lower than the ratio found in Ref. 36 in Fig. 7a, for a similar case with $\Delta_{1,ss,an}$ equal to 12.9%. This difference could be attributed to certain differences in parameters used here and in Ref. 36. It is worth noting that in Ref. 36, the method they used broke down for a case where $\Delta_{1,ss,an}$ is equal to 16.0%, which could also explain certain differences in results.

In Fig. 2, we can observe certain oscillations in the drop deformation that persist over time, even when we might expect them to have stopped. These oscillations could potentially be eliminated by optimizing the implementation of the equations in the OpenFOAM® software, such as using certain cell face values in the equations as described in Ref. 13. However, this was not the main focus of our paper, which instead aimed to initiate the EMFD field. Additionally, we noticed that certain oscillations were present in the case where ϕ_l was 0, indicating a possible connection to the starting solver, especially given the relatively high drop deformations previously observed with the unmodified solver (as reported in Ref. 14). Overall, our results suggest that the model presented in this paper can be utilized for simulations employing EHD's perfect dielectric model.

b. Comparison with the leaky dielectric model Another analytical equation can be found for comparison with the leaky dielectric model:[15,36]

$$\Delta_{1,ss,an} = \frac{9}{16}\frac{r_{1,t=0}\varepsilon_2}{\gamma}\left(\frac{|\mathbf{E_{mu}}|}{2+\sigma_1/\sigma_2}\right)^2\left[1+\left(\frac{\sigma_1}{\sigma_2}\right)^2 -2\frac{\varepsilon_1}{\varepsilon_2}+\frac{3}{5}\left(\frac{\sigma_1}{\sigma_2}-\frac{\varepsilon_1}{\varepsilon_2}\right)\left(\frac{2+3\mu_{f1}/\mu_{f2}}{1+\mu_{f1}/\mu_{f2}}\right)\right] \tag{32}$$

Magnetic permeabilities of both fluids were set to be equal to $10^{-100}\,\mathrm{H\,m^{-1}}$. The reason for using this value can be seen in the previous comparison.

The study examined the effect of the number of cells per starting drop diameter on $\Delta_{1,ss,an}$ when it is equal to 0.12, where the geometry's width and height were five times the starting drop diameter and radius, respectively. The average drop deformation was investigated for 24, 50, and 80 cells per diameter, resulting in 0.1274, 0.1074, and 0.1079, respectively. Since the difference between the last two values is less than 1.000%, 50 cells per diameter were chosen. This value is 2.5 times greater than the 20 cells per diameter of a spherically shaped object.

The study also analyzed the effect of the width and height of the geometry on $\Delta_{1,ss,an}$ when it is equal to 0.12. For widths and heights of 5, 6, 7, 8, and 9 times the starting drop diameter and radius, the average drop deformation was 0.1074, 0.1072, 0.1071, 0.1063, and 0.1064, respectively. Since the difference between the first and last value is less than 1.000%, the geometry with a width and height five times the starting drop diameter and radius, respectively, was used.

Fig. 3 illustrates a comparison between the obtained results and corresponding analytical predictions. The greatest $\Delta_{1,ss,an}$ showed a deviation from Eq. (32), which was expected because the analytical solution relied on linearized asymptotic analysis.[15] The exact method for

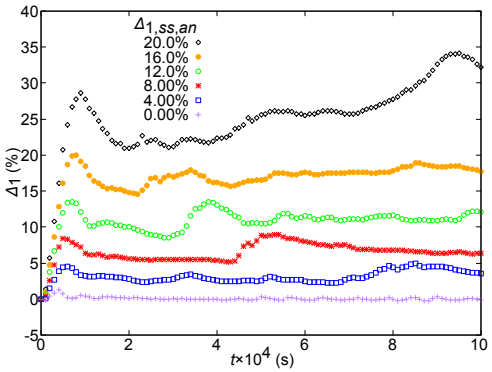

FIG. 3. Numerically obtained drop deformations for cases with different analytical predictions for comparison with the leaky dielectric model

calculating the correct divergence from this equation was not found. Despite this, the obtained drop deformations oscillated around the analytical value, even when the value was 16.0%. The model can be used for EHD's leaky dielectric model calculations, despite oscillations that may occur in the implementation. The oscillations' possible explanations are the same as in the previous comparison. In Ref. 15, their deformation value was higher than the one predicted analytically, even when the value was below 10%.

After conducting the analysis, it can be concluded that the model is suitable for calculations involving EHD's leaky dielectric model, despite possible oscillations.

2. *Three-dimensional cases*

Fig. 4 illustrates the geometry used in this study. To establish boundary conditions, $\nabla\phi$ was set to $\mathbf{0}$ on the top, bottom, front, and back borders, while ϕ was set to 0 on the left and right borders. In addition, $\nabla\rho_e$ was set to $\mathbf{0}$ on all borders. $\nabla\mathbf{A}$ was set to $\mathbf{0}$ on the left, right, front, and back borders. Due to asymmetry, an axially symmetric geometry could not be used for comparison.

The mesh comprised hexahedra with equal dimensions, and 24 cells per the starting drop diameter were used. This is 1.2 times greater than 20 cells per the diameter of a spherically shaped object. The computational heaviness of the simulations and the available computational resources limited the use of more cells per $d_{1,t=0}$ and a larger domain.

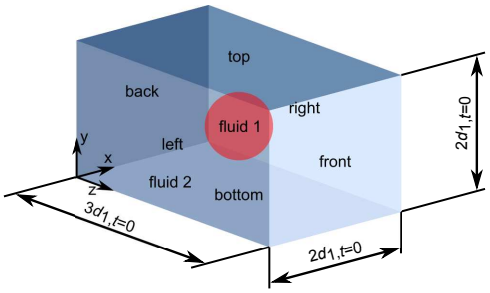

FIG. 4. An illustration of the three-dimensional geometry

a. Comparison with an MHD equation An analytical equation from MHD for a drop deformation caused by a magnetic field is given by:[18]

$$Bo_m = \left(\frac{\mu_2}{\mu_1 - \mu_2} + k\right)^2 \left(\frac{b}{a}\right)^{1/3} \left[2\frac{b}{a} - \left(\frac{b}{a}\right)^{-2} - 1\right] \tag{33}$$

where Bo represents the Bond number, and k represents the demagnetizing factor.

The following equation was used for the magnetic Bond number:[18]

$$Bo_m = \frac{\mu_2 |\mathbf{H_{mu}}|^2 r_{1,t=0}}{2\gamma} \tag{34}$$

The demagnetizing factor is calculated from:[18]

$$k = \left(\frac{1-\xi^2}{2\xi^3}\right)\left(\ln\frac{1+\xi}{1-\xi} - 2\xi\right) \tag{35}$$

where ξ is the eccentricity, which is calculated from:[18]

$$\xi = \sqrt{1 - a^2/b^2} \tag{36}$$

According to Ref. 18, Eq. (33) could have more than one solution. If we use $|\mathbf{H_{mu}}| = 11999\,\mathrm{A\,m^{-1}}$ and $b/a = 1.0905186$ in this equation (these values were obtained by using a nonlinear solver), the difference from zero that we can obtain is less than 10^{-9}. Therefore, we can consider a combination of these two values as one of the possible solutions.

We ran two simulations. In simulation 1, we set $\mathbf{A}$ to $\mathbf{0}$ on the top and bottom borders, while in simulation 2, we set it to $(1.235\times10^{-6},0,0)\,\mathrm{V\,s\,m^{-1}}$ on the top border and to $(-1.235\times10^{-6},0,0)\,\mathrm{V\,s\,m^{-1}}$ on the bottom border. We tried different boundary conditions for $\mathbf{A}$ on all

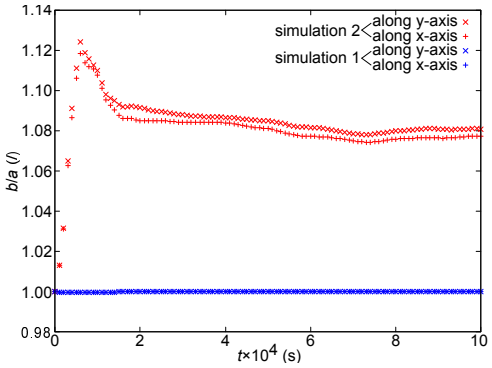

FIG. 5. Numerically obtained results for three-dimensional simulations

borders, but we found this combination to produce more uniform values of |**H**|. The results of the simulations are presented in Fig. 5, which shows that the model can simulate drop deformations caused by these boundary conditions. We measured the values of a along both the x- and the y-axis, and we found them to be somewhat different, which is expected since the borders were not symmetrical.

In Fig. 6, we present the calculated |**H**| on the front border at 10^{-5} s for simulation 2. The minimum value of |**H**|, which is farther away from the drop and not in the central ellipsoidal area, is 11999 A m^{-1}. From Fig. 5, we observed that b/a was around 1.08 after some time, while the analytically predicted value was 1.0905186. This result agrees with Eq. (33) and Ref. 18, but we might need simulations with a higher number of cells and different boundary conditions for a better comparison.

B. Electrospinning

Electrospinning is a process used to manufacture fibers and textiles.[24,27] In this process, a liquid flows out of a capillary tube in an electric field and forms a jet. It is different from the electrospraying process because droplet production is not the goal.[38] The diameter of the jet can be calculated using different analytical equations, depending on the position of the jet.[24] To determine the diameter of the jet far from the nozzle, the analytical equation in Ref. 39 is used:

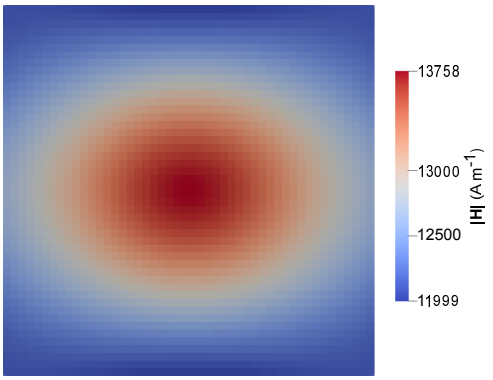

FIG. 6. |**H**| on the front border at 10^{-5} s for simulation 2

$$d_{j,an} = \left[\frac{2}{\pi^3}\frac{\rho_1 Q_{ct,1}^3 l_j}{\sigma_1 (\phi_{ct} - \phi_b)^2}\right]^{1/6} \tag{37}$$

where Q represents the volumetric flow rate, l represents the length, and subscripts j, ct, and b denote the jet, the capillary tube, and the bottom border, respectively.

In simulations, fluid 1 and fluid 2 have mass densities of 1410 kg m^{-3} and 1 kg m^{-3}, respectively. The kinematic viscosity of fluid 1 and fluid 2 is 1.41×10^{-3} m^2 s^{-1} and 1.48×10^{-3} m^2 s^{-1}, respectively, while the interfacial tension between the two fluids is 0.075 N m^{-1}. The gravitational acceleration has a downward direction and a value of 9.81 m s^{-2}. The electric permittivity is equal to 5×10^{-10} F m^{-1} and to 8.85×10^{-12} F m^{-1}, the electric conductivity is 1.08×10^{-7} S m^{-1} and 10^{-14} S m^{-1}, and the magnetic permeability is 1.25663×10^{-6} H m^{-1} and 1.25664×10^{-6} H m^{-1} for fluid 1 and fluid 2, respectively. The inlet speed of fluid 1 is 0.17 m s^{-1}. The capillary tube's inner diameter is 5×10^{-4} m, while the outer diameter is 6×10^{-4} m. The capillary tube's length that was simulated is equal to 10^{-3} m, while the distance between the capillary tube and the geometry's bottom is 2×10^{-2} m. The values chosen for the simulations are realistic for the electrospinning process.

Fig. 7 provides an illustration of the used axially symmetric geometry. The symmetry axis is located at the left border. The top-left border is the inlet of fluid 1. Fluid 1 can exit through the top-right, right, and bottom borders, while fluid 2 can both enter and exit. The other borders at the top of the geometry are walls that represent the capillary tube. At the beginning of the simulations, fluid 1 was exclusively in region IV, while fluid 2 was in other regions. The value of ϕ was constant and changed as needed at the top borders that represent the capillary tube, while it was set to 0 on

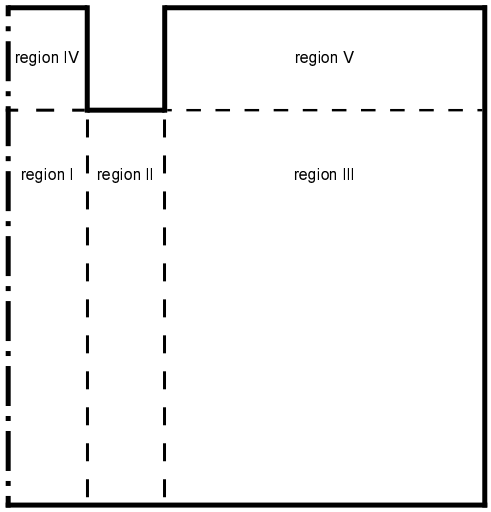

FIG. 7. An illustration of the axially symmetric geometry used for the electrospinning process (not in scale)

the bottom border. $\nabla\phi$ was set to $\mathbf{0}$ on the top-left, top-right, and right border. $\nabla\rho_e$ was set to $\mathbf{0}$ on all the top borders except the top-right border. On other borders, except the left border, $\nabla\rho_e$ was set to $\mathbf{0}$ in case of an outflow, while ρ_e was set to 0 in case of an inflow. $\mathbf{A}$ was set to $\mathbf{0}$ on the right border, and $\nabla\mathbf{A}$ to $\mathbf{0}$ on other borders, except the left border.

The mesh consisted of hexahedra and prisms. Grading was used for the width and the height of the cells to decrease simulation time. Great care was taken to make the borders of the mesh regions indiscernible. The ratio of the widths of the most left cell to the most right cell was equal to 1 for regions I, II, and IV, and to 1/10 for regions III and V. The ratio of the height of the cell that is on the region's top border and the cell that is on the bottom was equal to 1/5 for regions I–III, and to 5 for regions IV and V.

In order to reduce the time required for the simulations, a target maximum value of 0.8 was set for all Courant numbers. Additionally, the while loop that begins after Eq. (26) was configured to have 10 iterations or to terminate earlier if the tolerance and relative tolerance for ϕ, ρ_e, and $\mathbf{A}$ were less than those used in a single solving of the corresponding equation. The simulation was run for 0.8 s, with results outputted every 2×10^{-3} s. This value was also used for the maximum time step and as the initial value for the first time step. The value of $\overline{d_j}$ was determined by taking the time average value obtained from the results outputted between 0.4 s and the end of the simulation.

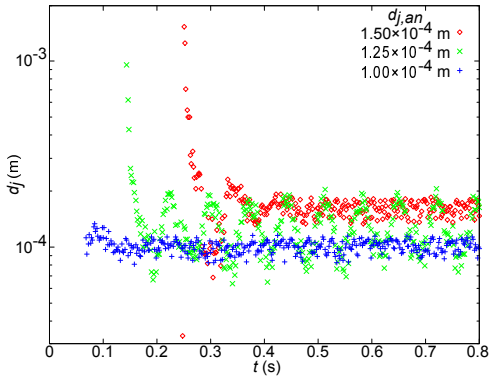

FIG. 8. Numerically obtained jet diameters for three cases with different analytical predictions

In this study, the impact of the width of the geometry on the obtained value of $\overline{d_j}$ was investigated. The width of the cells in region I was set to 5×10^{-5} m, while $d_{j,an}$ was 1.50×10^{-4} m. The geometry width was varied to be 10, 11, 12, and 13 times greater than the outer diameter of the capillary tube. The obtained $\overline{d_j}$ values were 1.678×10^{-4} m, 1.688×10^{-4} m, 1.696×10^{-4} m, and 1.693×10^{-4} m, respectively. The results showed that the difference between the value obtained when the width was 10 times greater and when it was 13 times greater was less than 1.000%. Thus, it was concluded that the geometry width 10 times greater than the outer diameter of the capillary tube was suitable for the study.

Furthermore, the study also investigated the impact of the size of the cells on the obtained value of $\overline{d_j}$, when $d_{j,an}$ was 1.25×10^{-4} m. The width of the cells in region I was tested at 5×10^{-5} m, 2.5×10^{-5} m and 5/3×10^{-5} m. The obtained $\overline{d_j}$ values were 1.421×10^{-4} m, 1.259×10^{-4} m, and 1.257×10^{-4} m, respectively. As the difference between the last two values was less than 1.000%, the width of the cells in region I was set to be 2.5×10^{-5} m. This mesh was found to have 2670, 534, 5340, 140, and 280 cells in region I, II, III, IV, and V, respectively.

In Fig. 8, we can see the values of the jet diameters that were obtained for three cases. The cause of the oscillations may be the same as in previous cases, but it is also possible that they were accurately predicted for the electrospinning process. This is because stretching and whipping of a jet can occur, as seen in Ref. 39. Moreover, the non-uniform size of fibers can be observed in laboratory experiments.[40] In Fig. 9, we can see the volume fraction of fluid 1 at the end of the simulation for the case when the value of $d_{j,an}$ was equal to 1.50×10^{-4} m.

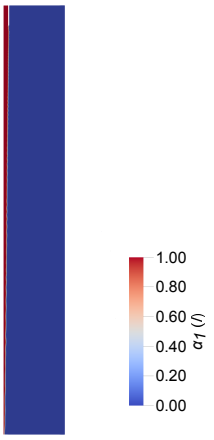

FIG. 9. The volume fraction of fluid 1 at 0.8 s for $d_{j,an} = 1.50 \times 10^{-4}$ m

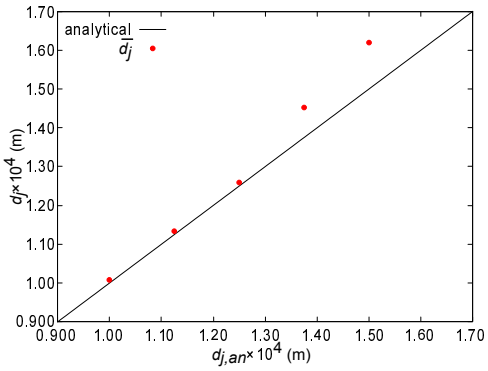

FIG. 10. Comparison with the analytical predictions for the electrospinning process

In Fig. 10, we compare the obtained values of $\overline{d_j}$ to $d_{j,an}$. It can be concluded that the obtained $\overline{d_j}$ was not almost equal to $d_{j,an}$ only for the two greatest values of $d_{j,an}$. This could be attributed to the electric field becoming too weak for Eq. (37) to be applicable. These results demonstrate that the model and its implementation are applicable for laboratory and industrial cases, even for complex flowing scenarios, and are close to analytical predictions. To our understanding, this is the first time that a model has been validated using this process and a corresponding analytical equation.[28]

IV. CONCLUSIONS

Electromagnetics and fluid dynamics have advanced sufficiently to establish the electro-magneto-fluid dynamics field. This paper derives equations for a two-phase EMFD model, which can be integrated into computational fluid dynamics software such as OpenFOAM®. The limitations of the software were overcome by deriving appropriate equations. The lack of single-phase EMFD models that can be integrated into CFD software is resolved with this model. This implies that the merging of electromagnetics and fluid dynamics can be expected, while future work on electrohydrodynamics and magnetohydrodynamics may be reduced.

To demonstrate the quality of the EMFD model, it was implemented and validated by comparing the results to analytical predictions from EHD and MHD. The obtained results were closer to the analytical predictions than those in the literature used for two models from EHD.[15,36] One simulation was compared to an analytical prediction from MHD[18], and showed good agreement. Finally, the electrospinning process was simulated and the results were close to analytical predictions. The EMFD model can be used for both EHD and MHD cases.

The presented model and its implementation can be used for both laboratory and industrial scale without any modification because there are no scale limitations for the electromagnetic expressions and because fluid dynamics (and OpenFOAM®) can be used for both laboratory and industrial scale without any modification. They can be further extended, improved, or analyzed in future work. Better handling of complex numbers and implicit solving of the gradient and the curl of a variable in CFD software might positively affect EMFD calculations. Therefore, the wide inclusion of the effects of electromagnetic fields on fluid flows in CFD software can be initiated based on this work. It can be expected that this model and this implementation could help with the usage of the electrospinning process and therefore be useful for the biomedical, energy, catalysis and other fields that are useful to the society.[28] Other potential uses could be discovered in future.

ACKNOWLEDGMENTS

This work was supported by the Ministry of Science, Technological Development and Innovation of the Republic of Serbia (Contracts No. 451-03-47/2023-01/200287 and No. 451-03-47/2023-01/200135) and by the Science Fund of the Republic of Serbia (The Program IDEAS MultiPromis 7751519).

AUTHOR DECLARATIONS

Conflict of interest

The authors have no conflicts to disclose.

Author contributions

Stefan A. Bošković: Conceptualization, Formal analysis, Investigation, Methodology, Resources, Software, Validation, Visualization, Writing – original draft, Writing – review & editing. **Branko Bugarski**: Funding acquisition, Project administration, Resources, Supervision, Writing – review & editing.

DATA AVAILABILITY STATEMENT

The data that supports the findings of this study are available from the corresponding author upon reasonable request.

REFERENCES

[1]G. S. Dulikravich and S. R. Lynn, "Unified electro-magneto-fluid dynamics (EMFD): Introductory concepts," Int. J. Non-Linear Mech. **32**, 913–922 (1997).

[2]R. S. Allan and S. G. Mason, "Particle behaviour in shear and electric fields. I. Deformation and burst of fluid drops," Proc. R. Soc. Lond. A **267**, 45–61 (1962).

[3]R. Thirumalaisamy, G. Natarajan, and A. Dalal, "Towards an improved conservative approach for simulating electrohydrodynamic two-phase flows using volume-of-fluid," J. Comput. Phys. **367**, 391–398 (2018).

[4]A. Shevchenko and M. Kaivola, "Electromagnetic force density and energy–momentum tensor in an arbitrary continuous medium," J. Phys. B: At., Mol. Opt. Phys. **44**, 175401 (2011).

[5]A. Shevchenko and M. Kaivola, "Electromagnetic force density in dissipative isotropic media," J. Phys. B: At., Mol. Opt. Phys. **44**, 065403 (2011).

[6]M. Abraham, "Zur Elektrodynamik bewegter Körper," Rend. Circ. Matem. Palermo **28**, 1 (1909).

[7]H. Minkowski, "Die Grundgleichungen für die elektromagnetischen Vorgänge in bewegten Körpern," Nachr. Ges. Wiss. Göttingen **1908**, 53–111 (1908).

[8]A. Einstein and J. Laub, "Über die im elektromagnetischen Felde auf ruhende Körper ausgeübten ponderomotorischen Kräfte," Ann. Phys. (Berl.) **331**, 541–550 (1908).

[9]A. Shevchenko and B. J. Hoenders, "Microscopic derivation of electromagnetic force density in magnetic dielectric media," New J. Phys. **12**, 053020 (2010).

[10]N. C. Lima and M. A. d'Ávila, "Numerical simulation of electrohydrodynamic flows of Newtonian and viscoelastic droplets," J. Non-Newtonian Fluid Mech. **213**, 1–14 (2014).

[11]E. Çolak, H. F. Öztop, and Ö. Ekici, "MHD mixed convection in a chamfered lid-driven cavity with partial heating," Int. J. Heat Mass Tran. **156**, 119901 (2020).

[12]S. Sander, S. Gawor, and U. Fritsching, "Separating polydisperse particles using electrostatic precipitators with wire and spiked-wire discharge electrode design," Particuology **38**, 10–17 (2018).

[13]S. A. Bošković, A. Karač, S. B. Vrhovac, A. Belić, and B. Bugarski, "Investigation of electrohydrodynamic calculations," Hem. Ind. **76**, 65–74 (2022).

[14]S. A. Bošković, A. Karač, S. B. Vrhovac, A. Belić, and B. Bugarski, "Implementation of the electrohydrodynamics' perfect dielectric model in OpenFOAM®," J. Eng. Process. Manag. **14**, 66–75 (2022).

[15]J. M. López-Herrera, S. Popinet, and M. A. Herrada, "A charge-conservative approach for simulating electrohydrodynamic two-phase flows using volume-of-fluid," J. Comput. Phys. **230**, 1939–1955 (2011).

[16]G. I. Taylor, "Studies in electrohydrodynamics. I. The circulation produced in a drop by an electric field," Proc. R. Soc. Lond. A **291**, 159–166 (1966).

[17]D. Das and D. Saintillan, "A three-dimensional small-deformation theory for electrohydrodynamics of dielectric drops," J. Fluid Mech. **914**, A22 (2021).

[18]S. Afkhami, A. J. Tyler, Y. Renardy, M. Renardy, T. G. S. Pierre, R. C. Woodward, and J. S. Riffle, "Deformation of a hydrophobic ferrofluid droplet suspended in a viscous medium under uniform magnetic fields," J. Fluid Mech. **663**, 358–384 (2010).

[19]M. N. Shneider and M. Pekker, "Dielectric fluid in inhomogeneous pulsed electric field," Phys. Rev. E **87**, 043004 (2013).

[20]F. Moukalled, L. Mangani, and M. Darwish, *The Finite Volume Method in Computational Fluid Dynamics: An Advanced Introduction with OpenFOAM® and Matlab®* (Springer International

Publishing Switzerland, Switzerland, 2016).

[21]C. R. Maliska, *Fundamentals of Computational Fluid Dynamics: The Finite Volume Method* (Springer Nature Switzerland AG, Cham, Switzerland, 2023).

[22]B. Andersson, R. Andersson, L. Håkansson, M. Mortensen, R. Sudiyo, B. van Wachem, and L. Hellstrom, *Computational Fluid Dynamics for Engineers* (Cambridge University Press, Cambridge, UK, 2012).

[23]A. Ionescu, ed., *Computational Fluid Dynamics: Basic Instruments and Applications in Science* (InTech, Rijeka, Croatia, 2018).

[24]S. Bošković and B. Bugarski, "Review of electrospray observations and theory," J. Eng. Process. Manag. **10**, 41–53 (2018).

[25]B. Bugarski, Q. Li, M. F. A. Goosen, D. Poncelet, R. J. Neufeld, and G. Vunjak, "Electrostatic droplet generation: Mechanism of polymer droplet formation," AIChE J. **40**, 1026–1031 (1994).

[26]T. He and J. V. Jokerst, "Structured micro/nano materials synthesized via electrospray: a review," Biomater. Sci. **8**, 5555–5573 (2020).

[27]A. Vaseashta and N. Bölgen, eds., *Electrospun Nanofibers: Principles, Technology and Applications* (Springer Nature Switzerland AG, Cham, Switzerland, 2022).

[28]Y. Guo, X. Wang, Y. Shen, K. Dong, L. Shen, and A. A. A. Alzalab, "Research progress, models and simulation of electrospinning technology: a review," J. Mater. Sci. **57**, 58–104 (2022).

[29]N. C. Lima, *Numerical Studies in Electrohydrodynamics*, phdthesis, School of Mechanical Engineering of the University of Campinas (2017).

[30]Q. Nie, Q. Ma, W. Yang, X. Pan, Z. Liu, H. Fang, and Z. Yin, "Designing working diagrams for electrohydrodynamic printing," Chem. Eng. Sci. **240**, 116661 (2021).

[31]K. Ó. Klausen, *A Treatise on the Magnetic Vector Potential* (Springer Nature Switzerland AG, Cham, Switzerland, 2020).

[32]C. S. Adams and I. G. Hughes, *Optics f2f: From Fourier to Fresnel* (Oxford University Press, New York, New York, USA, 2019).

[33]D. B. Melrose and R. C. McPhedran, *Electromagnetic processes in dispersive media* (Cambridge University Press, New York, USA, 1991).

[34]N. Weber, V. Galindo, F. Stefani, T. Weier, and T. Wondrak, "Numerical simulation of the Tayler instability in liquid metals," New J. Phys. **15**, 043034 (2013).

[35]E. Robertson, V. Choudhury, S. Bhushan, and D. K. Walters, "Validation of OpenFOAM numerical methods and turbulence models for incompressible bluff body flows," Comput. Fluids

123, 122–145 (2015).

[36]G. Supeene, C. R. Koch, and S. Bhattacharjee, "Deformation of a droplet in an electric field: Nonlinear transient response in perfect and leaky dielectric media," J. Colloid Interface Sci. **318**, 463–476 (2008).

[37]R. Singh, S. S. Bahga, and A. Gupta, "Electrohydrodynamics in leaky dielectric fluids using lattice Boltzmann method," Eur. J. Mech. B. Fluids **74**, 167–179 (2019).

[38]D. Poncelet, R. J. Neufeld, M. F. A. Goosen, B. Burgarski, and V. Babak, "Formation of microgel beads by electric dispersion of polymer solutions," AIChE J. **45**, 2018–2023 (1999).

[39]B. Cramariuc, R. Cramariuc, R. Scarlet, L. R. Manea, I. G. Lupu, and O. Cramariuc, "Fiber diameter in electrospinning process," J. Electrostat. **71**, 189–198 (2013).

[40]A. Salević, D. Stojanović, S. Lević, M. Pantić, V. Đorđević, R. Pešić, B. Bugarski, V. Pavlović, P. Uskoković, and V. Nedović, "The Structuring of Sage (Salvia officinalis L.) Extract-Incorporating Edible Zein-Based Materials with Antioxidant and Antibacterial Functionality by Solvent Casting versus Electrospinning," Foods **11**, 390 (2022).